IJMMM International Journal of Minerals, Metallurgy and Materials 矿物冶金与材料学报（英文版）

# Fabrication and performance of 3D co-continuous magnesium composites reinforced with $Ti_2AlN_x$ MAX phase

Wantong Chen, Wenbo Yu, Pengcheng Zhang, Xufeng Pi, Chaosheng Ma, Guozheng Ma, and Lin Zhang

Cite this article as:

Wantong Chen, Wenbo Yu, Pengcheng Zhang, Xufeng Pi, Chaosheng Ma, Guozheng Ma, and Lin Zhang, Fabrication and performance of 3D co-continuous magnesium composites reinforced with $Ti_2AlN_x$ MAX phase, *Int. J. Miner. Metall. Mater.*, 29(2022), No. 7, pp. 1406-1412. https://doi.org/10.1007/s12613-022-2427-2

View the article online at SpringerLink or IJMMM Webpage.

---

*International Journal of Minerals, Metallurgy and Materials*
*Volume 29, Number 7, July 2022, Page 1406*
https://doi.org/10.1007/s12613-022-2427-2

# Fabrication and performance of 3D co-continuous magnesium composites reinforced with $Ti_2AlN_x$ MAX phase

*Wantong Chen*[1)], *Wenbo Yu*[1),✉], *Pengcheng Zhang*[1)], *Xufeng Pi*[1)], *Chaosheng Ma*[1)], *Guozheng Ma*[2)], *and Lin Zhang*[3)]

1) Center of Materials Science and Engineering, School of Mechanical and Electronic Control Engineering, Beijing Jiaotong University, Beijing 100044, China
2) National Key Lab for Remanufacturing, Army Academy of Armored Forces, Beijing 100072, China
3) China Academy of Machinery Science and Technology Group Co., Ltd., Beijing 100044, China
(Received: 7 September 2021; revised: 23 January 2022; accepted: 25 January 2022)

**Abstract:** Magnesium composites reinforced by N-deficient $Ti_2AlN$ MAX phase were first fabricated by non-pressure infiltration of Mg into three-dimensional (3D) co-continuous porous $Ti_2AlN_x$ ($x$ = 0.9, 1.0) preforms. The relationship between their mechanical properties and microstructure is discussed with the assessment of 2D and 3D characterization. X-ray diffraction (XRD) and scanning electron microscopy detected no impurities. The 3D reconstruction shows that the uniformly distributed pores in $Ti_2AlN_x$ preforms are interconnected, which act as infiltration tunnels for the melt Mg. The compressive yield strength and microhardness of $Ti_2AlN_{0.9}$/Mg are 353 MPa and 1.12 GPa, respectively, which are 8.55% and 6.67% lower than those of $Ti_2AlN$/Mg, respectively. The typical delamination and kink band occurred in $Ti_2AlN_x$ under compressive and Vickers hardness ($V_H$) tests. Owing to the continuous skeleton structure and strong interfacial bonding strength, the crack initiated in $Ti_2AlN_x$ was blocked by the plastic Mg matrix. This suggests the possibility of regulating the mechanical performance of $Ti_2AlN$/Mg composites by controlling the N vacancy and the hierarchical structure of $Ti_2AlN$ skeleton.

**Keywords:** $Ti_2AlN$; magnesium matrix composites; co-continuous structure; N vacancy

## 1. Introduction

Due to the increasing requirement of lightweight products in the industrial, including aerospace, automotive, and electronics industries, the demand for lightweight magnesium components is increasing [1–4]. However, to meet the demands of some applications, such as motor pulleys and engine blocks, ceramic particles must be introduced into the Mg matrix to enhance the matrix stiffness and wear resistance [5].

Recently, a novel ternary nanolayered MAX phase ($M_{n+1}AX_n$, where M is an early transition metal, A belongs to group IIIA or IVA, X is C and/or N, and $n$ = 1−3) that exhibits metal and ceramic-like properties gained attention [6–7]. Different from traditional reinforcements, such as TiC, SiC, $B_4C$, graphite, and $Al_2O_3$ [8–11], Al elements can diffuse out from MAX phases at a certain temperature due to the low migration energy of Al in Al-contained MAX phases [12–13]. This can produce a strong interface between Al-contained MAX phases and the Mg matrix. For example, Yu *et al.* [14] and Amini *et al.* [15] experimentally observed the formation of a robust amorphous interfacial layer and nanosize Mg grains among $Ti_2AlC$ particles. Anasori *et al.* [16] found that 20vol% $Ti_2AlC$-reinforced Mg composite obtained by power metallurgy could dissipate 30% mechanical energy during each compressive load at 250 MPa. In addition, Yu *et al.* [17–18] found that the high damping capacity and superior self-lubricating capacity of $Ti_2AlC$ were attributed to its high dislocation density and graphite-like layered structure. However, the distribution of MAX phases in the Mg matrix is discontinuous in all the composites fabricated by semi-solid stir casting and powder metallurgy reported in the literature [14–15].

There has been no relevant research on the three-dimensional (3D) continuous network magnesium composite reinforced by MAX phases. According to the literature [19–20], the 3D continuous network that is composed of a ceramic skeleton and metal skeleton exhibits high load-bearing and thermal shock resistance performance. The metal skeleton transfers and disperses stress, whereas the ceramic skeleton efficiently improves the stiffness of the metal matrix. The interlocking effect of this structure endows the material's excellent damage tolerance and low risk of failure [21–22]. Investigations reveal that co-continuous ceramic–metal composites prepared by the infiltration method exhibit excellent mechanical properties [21,23–25]. For example, co-continuous $TiC_x/Cu–Cu_4Ti$ composites produced by infiltrating the melting Cu into $TiC_{0.5}$ porous ceramic preforms exhibited an

✉ Corresponding author: Wenbo Yu E-mail: wbyu@bjtu.edu.cn

excellent thermal shock resistance and good mechanical properties [21]. Wang *et al*. [23] reported that co-continuous $Ti_3AlC_2$/Al composites produced by pressureless infiltration could maintain their good mechanical properties at relatively high temperatures. Furthermore, Yu *et al*. [26] reported that mechanical properties of $Ti_2AlN_x$ can be modified by controlling the vacancy of N. The elastic modulus and intrinsic hardness of $Ti_2AlN$ increase with the increased N content. This suggests that the regulation of the mechanical performance of the $Ti_2AlN$/Mg composite is possible by controlling the N content in $Ti_2AlN$ instead of regulating the $Ti_2AlN$ content in the Mg matrix.

On the basis of the abovementioned points, the *in-situ* formed porous $Ti_2AlN_x$ ($x$ = 0.9, 1) preforms were infiltrated by pure magnesium in this work. To investigate the relationship between their mechanical properties and their microstructure, 2D and 3D characterizations were conducted.

## 2. Experimental

### 2.1. Fabrication process

As shown in Fig. 1, starting powders of Ti, Al, and TiN (purity ≥99%, particle size 300 mesh) were mixed with molar ratios of 2Ti : 1.05Al : 0.9N and 2Ti : 1.05Al : 1.0N to prepare $Ti_2AlN_{0.9}$ and $Ti_2AlN$ preforms. The mixed powders were first compressed into a green body under an axial pressure of 40 MPa. Thereafter, the green body was put into a graphite die coated with BN and sintered in a vacuum sintering furnace at 1400°C in 20 min under Ar gas. Note that the powder mixtures used in this study contain an excess of 5at% of Al to compensate the loss of aluminum by preferential out-diffusion during the sintering process [26]. The obtained porous $Ti_2AlN_x$ preforms that were sandwiched between two Mg cylinder blocks were then heated to 750°C in 90 min in an $Al_2O_3$ crucible under Ar gas, which was followed by the furnace cooling to room temperature.

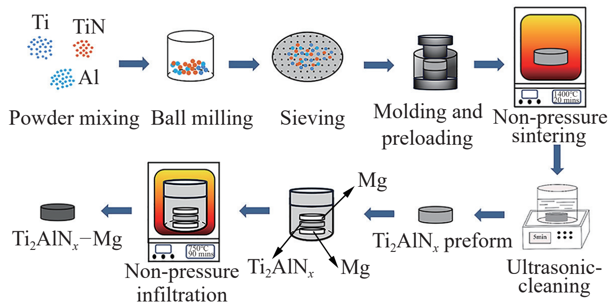


**Fig. 1. Fabrication procedure of $Ti_2AlN_x$–Mg composites.**

### 2.2. Microstructure characterization

Phase identification was performed by X-ray diffraction (XRD) using a Bruker (Karlsruhe, Germany) D8 diffractometer with Cu $K_\alpha$ radiation. Wavelength dispersive X-ray spectroscopy (WDS, CAMECA SX100) was used to determine the chemical composition of $Ti_2AlN_x$. The microstructural observation was performed by scanning electron microscopy (SEM, Merlin). Synchrotron X-ray micro-tomography experiments were conducted at the BL13W1 beamline with an X-ray energy of 36 keV at the Shanghai Synchrotron Radiation Facility to reconstruct the 3D real structure. The exposure time was set as 1 s using the Hamamatsu Flash 4.0 camera. The 4X lens was selected and the voxel size was 1.625 $\mu m^3$. The data was reconstructed by a phase retrieval algorithm in the PITRE software and a 3D microstructure was acquired using the AVISO software. Based on 3D reconstruction, $Ti_2AlN_x$ volumes were extracted and summarized in Table 1. In addition, densities of the composites were measured using Archimedes' principle.

**Table 1. Material characterization results obtained from composites**

| Material | Volume fraction of $Ti_2AlN_x$ | Bulk density / ($g \cdot cm^{-3}$) | Relative density / % |
|---|---|---|---|
| $Ti_2AlN_{0.9}$–Mg | 55% | 3.06 ± 0.02 | 97.03 |
| $Ti_2AlN_{1.0}$–Mg | 54% | 3.09 ± 0.02 | 98.79 |

### 2.3. Mechanical test

Uniaxial compressive tests were performed on specimens with a diameter of 5 mm and a height of 8 mm on a universal servo-hydraulic mechanical testing machine with a strain rate of 0.5 mm/min at room temperature in air. Microhardness measurements were carried out using a Vickers microindenter at loads of 10, 30, 50, 100, and 200 N and were held for 15 s. Each test was repeated five times for each composite to evaluate its mechanical properties.

## 3. Results and discussion

### 3.1. Microstructure of $Ti_2AlN$ preforms and their composites

The backscattered 2D images of $Ti_2AlN_{0.9}$ and $Ti_2AlN_{1.0}$ preforms are shown in Fig. 2(a–d). Both preforms are characterized by a uniform distribution of pores. In enlarged areas (Fig. 2(b) and (d)), the grain size of the $Ti_2AlN_{0.9}$ preform is bigger than that of $Ti_2AlN$. This phenomenon was also reported in our previous study of the $Ti_2AlN$ MAX phase [26], in which the grain size of $Ti_2AlN$ decreased with the increasing N content in starting powders. Furthermore, the absence of contrast in the images obtained under the backscattered mode suggests that the fabricated performs are pure. Fig. 2(e–h) presents the microstructure of $Ti_2AlN_{0.9}$/Mg and $Ti_2AlN$/Mg composites. It is evident that light-gray $Ti_2AlN_x$ phases and dark-gray Mg matrix are uniformly interlaced. Moreover, XRD analysis in Fig. 3 reveals that no other detectable trace appears except $Ti_2AlN$ and Mg. The sharp and clear interface in backscatter electron micrographs (Fig. 2(e–h)) confirms that no chemical reaction happened between $Ti_2AlN_x$ and Mg.

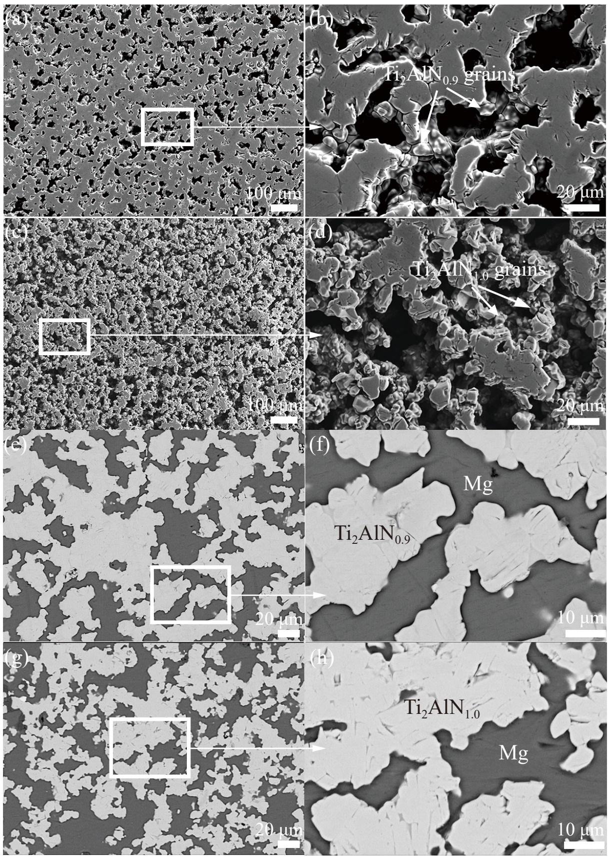


**Fig. 2. Backscattered (BSD) scanning micrographs of $Ti_2AlN$ preforms and its Mg composites: (a, b) $Ti_2AlN_{0.9}$ preform, (c, d) $Ti_2AlN_{1.0}$ preform, (e, f) $Ti_2AlN_{0.9}$/Mg composite, and (g, h) $Ti_2AlN_{1.0}$/Mg composites.**

$Ti_2AlN_x$ skeletons (Fig. 4(a) and (c)) and the corresponding infiltrated Mg (Fig. 4(b) and (d)) were extracted from the 3D reconstruction to reveal the 3D information of $Ti_2AlN_{0.9}$/Mg and $Ti_2AlN$/Mg composites. They are clearly characterized by a 3D co-continuous structure without fragmentation. Marked areas in Fig. 4(a–d) were respectively enlarged. The enlarged areas in Fig. 4(a) and (c) indicate that holes in $Ti_2AlN_x$ preforms are interconnected. Thus, the melt Mg could facilitate the infiltration of $Ti_2AlN_x$ preforms and form the three-dimensionally interconnected Mg network found in Fig. 4(b–d).

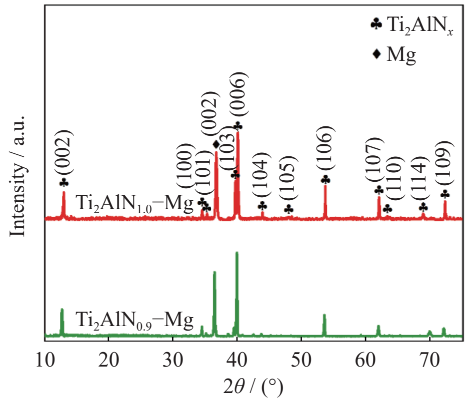


**Fig. 3. X-ray diffraction (XRD) diffractograms of $Ti_2AlN_{0.9}$/Mg and $Ti_2AlN_{1.0}$/Mg composites.**

### 3.2. Mechanical properties

Table 2 summarizes the compressive strength and microhardness of $Ti_2AlN_x$/Mg composites. The compressive yield strength and microhardness of $Ti_2AlN_{0.9}$/Mg are 353 MPa and 1.12 GPa, respectively, which are 8.55% and 6.67% lower than those obtained from $Ti_2AlN$/Mg, respectively (compressive yield strength = 386 MPa, microhardness = 1.20 GPa). However, the ultimate compressive strength of $Ti_2AlN_{0.9}$/Mg (395 MPa) is 3.66% lower than that of

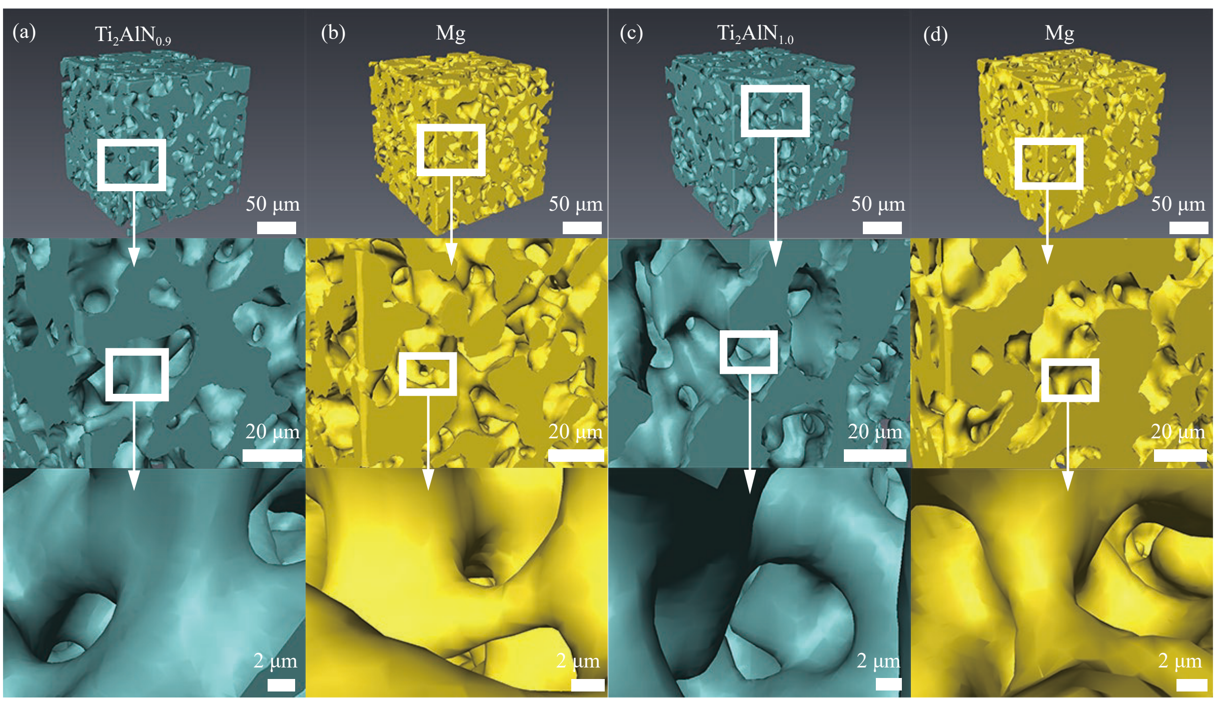


**Fig. 4. 3D reconstructed images of $Ti_2AlN_x$/Mg composites: (a) $Ti_2AlN_{0.9}$ skeleton, (b) Mg in $Ti_2AlN_{0.9}$/Mg composite, (c) $Ti_2AlN_{1.0}$ skeleton, and (d) Mg in $Ti_2AlN_{1.0}$/Mg composite.**

**Table 2. Compressive properties of different composites, including the 0.2% compressive yield strength ($\sigma_{0.2}$), compressive strength ($\sigma_f$), compressive fracture strain ($\varepsilon_f$), and Vickers hardness ($V_H$)**

| Material | $\sigma_{0.2}$ / MPa | $\sigma_f$ / MPa | $\varepsilon_f$ / % | $V_H$ / GPa |
|---|---|---|---|---|
| $Ti_2AlN_{0.9}$–Mg | 353 | 395 ± 7 | 14.4 | 1.12 |
| $Ti_2AlN_{1.0}$–Mg | 386 | 410 ± 8 | 13.1 | 1.20 |

$Ti_2AlN$/Mg (410 MPa). The yield strength is known to be proportional to Vickers hardness ($V_H$) for most materials [27–29]. These two composites have almost the same $Ti_2AlN_x$ volume and density with only a difference in the N content and grain of $Ti_2AlN_x$. Our previous study about bulk $Ti_2AlN_x$ revealed that the N deficiency in $Ti_2AlN_x$ leads to the reduction of the intrinsic hardness [26]. The hardness obtained from nanoindentation decreases from 9.7 GPa of $Ti_2AlN_{1.0}$ to 8.1 GPa of $Ti_2AlN_{0.9}$. Furthermore, the grain size effect is found in MAX phases [30–32]. For example, the $V_H$ values of coarse-grained (35 μm) and fine-grained (2 μm) $Cr_2AlC$ are 3.5 and 6.4 GPa [30]. In this work, the grain sizes of $Ti_2AlN_{0.9}$ and $Ti_2AlN$ (Fig. 2) are 12 and 6 μm, respectively. Here, the reduction of the compressive yield strength and microhardness in $Ti_2AlN_x$/Mg should be attributed to the grain size and N vacancy in $Ti_2AlN$. However, the 3D network ceramic and metal skeletons could efficiently transfer the load between each other. Due to this cooperative effect, the grain size and N vacancy effect are weakened in the ultimate compressive strength between $Ti_2AlN_{0.9}$ and $Ti_2AlN$. In addition, results show that the $Ti_2AlN$ ternary nanolayered MAX phase-reinforced magnesium matrix composites exhibit higher compressive yield strength and ultimate compressive strength than the reported binary nitride reinforcement, such as the AlN/Mg composite with 93 and 313 MPa, respectively [33].

Fig. 5 presents the indents of $Ti_2AlN_x$/Mg composites obtained under 50 N. No cracks propagated at the corners of indents for both composites. In the enlarged images, cracks appeared in $Ti_2AlN_x$ MAX phases rather than at the interface. This means that the strong interfacial bonding strength and the plastic Mg matrix can block the crack propagation in this continuous skeleton structure. In contrast, more cracks were found in $Ti_2AlN$/Mg, as shown in Fig. 5(c) and (d). It is known that hardness and ductility are often mutually exclusive [34]. Our previous work shows that the elastic modulus and intrinsic hardness of substoichiometric $Ti_2AlN_{0.9}$ are 268 and 8.1 GPa, respectively, which are smaller than those of $Ti_2AlN$ (elastic modulus = 278 GPa, intrinsic hardness = 9.7 GPa, respectively), obtained by nanoindentation [26]. Therefore, $Ti_2AlN$/Mg exhibits higher hardness and lower ductility, resulting in more cracks, which means the hardness and ductility of $Ti_2AlN_x$ affect the mechanical behavior of composites.

For all composites, the fracture occurred 45° with respect to the compression loading axis. As shown in Fig. 6, the cylindrical side of $Ti_2AlN$/Mg after the compressive test was carefully observed. The enlarged area that is shown in Fig. 6(b) indicates that some tiny lines appeared in $Ti_2AlN$ grains, far from the fracture line. However, Fig. 6(d) shows that no tiny line appeared in the untested $Ti_2AlN$/Mg composite. This difference suggests that $Ti_2AlN_x$/Mg specimens participated

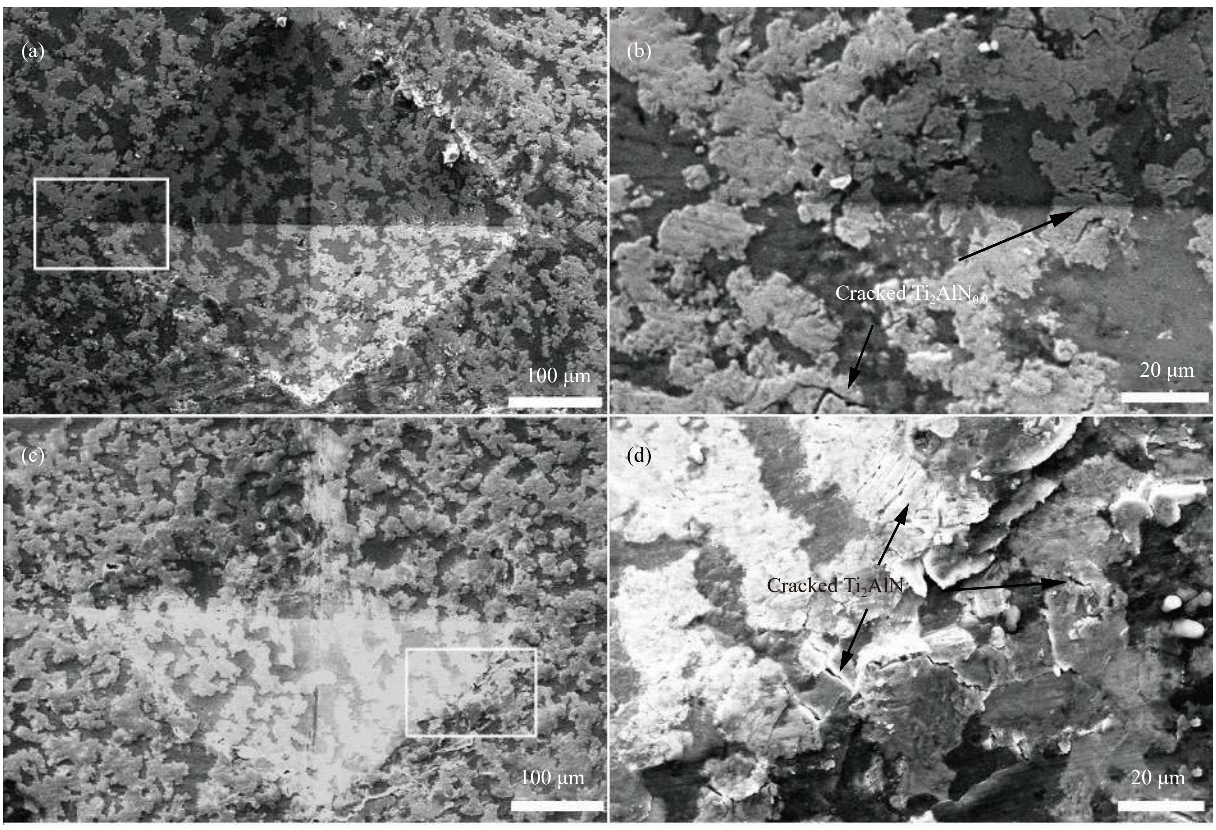


**Fig. 5. Microstructural morphologies of indents formed under 50 N: (a, b) $Ti_2AlN_{0.9}$/Mg composite; (c, d) $Ti_2AlN_{1.0}$/Mg composite.**

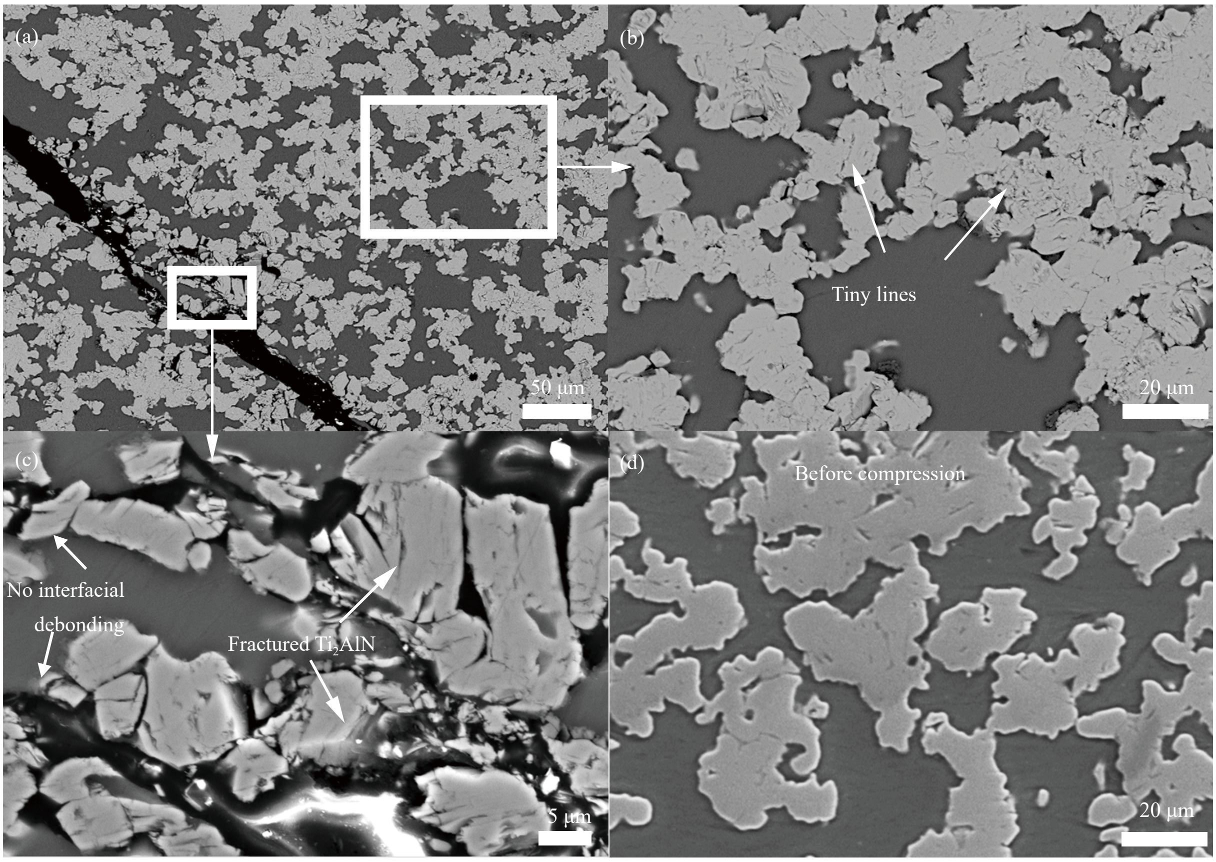


**Fig. 6. Backscattered images of the cylindrical side of $Ti_2AlN$–Mg (a–c) after and (d) before the compressive test.**

in deformation during the compressive test. Close to the fracture line, the enlarged area shown in Fig. 6(c) indicates that no interfacial decohesion happened between $Ti_2AlN$ and the Mg matrix. Meanwhile, some $Ti_2AlN$ particles fractured. This phenomenon is also found in our previous study about the $Ti_2AlC$/Mg composite because the interfacial bonding strength between $Ti_2AlC$ and Mg is higher than the Ti–Al bonding strength in the $Ti_2AlC$ MAX phase [14]. Electron energy-loss spectroscopy and band structure calculations reveal that there is only one very weak perturbation on the electronic structure when C is replaced by N in $Ti_2AlC$/N MAX phases [35]. The interface structure between $Ti_2AlN$ and Mg should be similar to that of $Ti_2AlC$ and Mg. Here, similar to $Ti_2AlC$/ Mg composites, no interfacial debonding occurred.

Fig. 7 indicates compressive fracture surfaces of specimens after compressive tests. For two composites, Fig. 7(a)

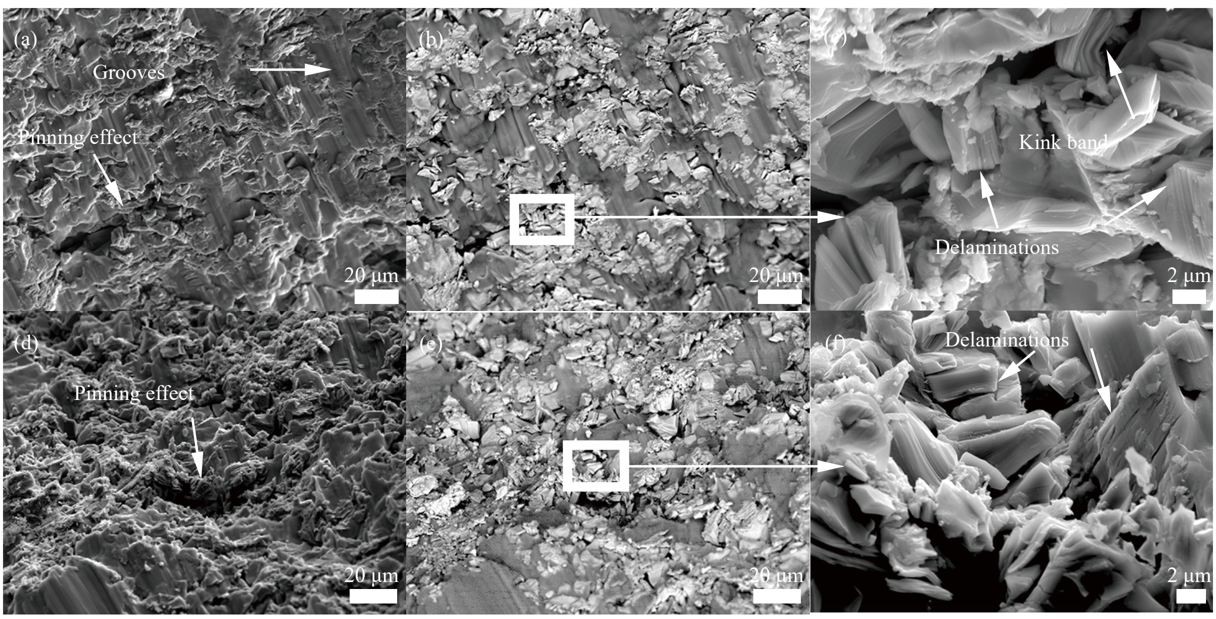


**Fig. 7. Compressive fracture morphologies of (a–c) $Ti_2AlN_{0.9}$–Mg and (d–f) $Ti_2AlN$–Mg composites. (a) and (d) are in SEM mode and the rest are in BSE mode.**

and (d) reveals that the rough fracture surface was characterized by some tiny grooves. In the corresponding backscattered mode, Fig. 7(b) and (e) indicates that $Ti_2AlN$ and Mg are uniformly distributed. There is no accumulation of MAX phases in the glide direction. This is different from composites from the semi-solid casting method and powder metallurgy, in which a seriously torn zone often appeared above the accumulated MAX phases in its reinforced metal composites [14,36]. The enlarged areas in Fig. 7(c) and (f) reveal that typical kink bands with very sharp radii of curvature or typical MAX phases delamination occurred in all $Ti_2AlN$ grains. Thus, these results prove that both $Ti_2AlN$ and Mg participated in the deformation during the compressive test due to their unique three-dimensional co-continuous network structure.

## 4. Conclusion

Through non-pressure infiltration, 3D co-continuous magnesium composites reinforced by $Ti_2AlN_x$ ($x$ = 0.9, 1.0) were successfully fabricated. Uniformly distributed holes in $Ti_2AlN_x$ preforms are interconnected without fragmentation. It is found that N vacancy and grain size effect in $Ti_2AlN_x$ lead to the reduction of the mechanical properties of composites, especially the yield compressive strength (YCS) and microhardness. The YCS and microhardness of $Ti_2AlN_{0.9}$/Mg are 353 MPa and 1.12 GPa, respectively, which were 8.55% and 6.67% lower than those obtained from $Ti_2AlN$/Mg, respectively. Due to the continuous skeleton structure and strong interfacial bonding strength, the crack initiated in $Ti_2AlN_x$ was blocked by the plastic Mg matrix. Moreover, the compressive fracture observation indicates that no interfacial decohesion occurred, and both $Ti_2AlN$ and Mg efficiently participated in the deformation with the delamination of $Ti_2AlN$ phases and severe plastic deformation of Mg. Therefore, this study demonstrates that it is possible to regulate the mechanical performance of $Ti_2AlN$/Mg composites by controlling the N vacancy in $Ti_2AlN$ other than the reinforcement content of $Ti_2AlN$ in the Mg matrix.


## Acknowledgements

This work was financially supported by the National Natural Science Foundation of China (No. 52175284), the State Key Lab of Advanced Metals and Materials (No. 2021-ZD08), and the Beijing Government Funds for the Constructive Project of Central Universities (No. 353139535).


## Conflict of Interest

The authors declare no potential conflict of interest.

## References


[1] M.O. Pekguleryuz and A.A. Kaya, Creep resistant magnesium alloys for powertrain applications, *Adv. Eng. Mater.*, 5(2003), No. 12, p. 866.

[2] V.E. Bazhenov, A.V. Koltygin, M.C. Sung, S.H. Park, Y.V. Tselovalnik, A.A. Stepashkin, A.A. Rizhsky, M.V. Belov, V.D. Belov, and K.V. Malyutin, Development of Mg–Zn–Y–Zr casting magnesium alloy with high thermal conductivity, *J. Magnes. Alloys*, 9(2021), No. 5, p. 1567.

[3] Y. Yang, X.M. Xiong, J. Chen, X.D. Peng, D.L. Chen, and F.S. Pan, Research advances in magnesium and magnesium alloys worldwide in 2020, *J. Magnes. Alloys*, 9(2021), No. 3, p. 705.

[4] X.P. Zhang, H.X. Wang, L.P. Bian, S.X. Zhang, Y.P. Zhuang, W.L. Cheng, and W. Liang, Microstructure evolution and mechanical properties of Mg–9Al–1Si–1SiC composites processed by multi-pass equal-channel angular pressing at various temperatures, *Int. J. Miner. Metall. Mater.*, 28(2021), No. 12, p. 1966.

[5] K.B. Nie, X.J. Wang, K.K. Deng, X.S. Hu, and K. Wu, Magnesium matrix composite reinforced by nanoparticles—A review, *J. Magnes. Alloys*, 9(2021), No. 1, p. 57.

[6] M.W. Barsoum, A. Murugaiah, S.R. Kalidindi, and T. Zhen, Kinking nonlinear elastic solids, nanoindentations, and geology, *Phys. Rev. Lett.*, 92(2004), No. 25, art. No. 255508.

[7] M.W. Barsoum, The $M_{N+1}AX_N$ phases: A new class of solids: Thermodynamically stable nanolaminates, *Prog. Solid State Chem.*, 28(2000), No. 1-4, p. 201.

[8] X.J. Wang, K. Wu, W.X. Huang, H.F. Zhang, M.Y. Zheng, and D.L. Peng, Study on fracture behavior of particulate reinforced magnesium matrix composite using *in situ* SEM, *Compos. Sci. Technol.*, 67(2007), No. 11-12, p. 2253.

[9] B. Inem and G. Pollard, Interface structure and fractography of a magnesium-alloy, metal-matrix composite reinforced with SiC particles, *J. Mater. Sci.*, 28(1993), No. 16, p. 4427.

[10] G.H. Majzoobi and K. Rahmani, Mechanical characterization of Mg–$B_4C$ nanocomposite fabricated at different strain rates, *Int. J. Miner. Metall. Mater.*, 27(2020), No. 2, p. 252.

[11] H.M. Xia, L. Zhang, Y.C. Zhu, N. Li, Y.Q. Sun, J.D. Zhang, and H.Z. Ma, Mechanical properties of graphene nanoplatelets reinforced 7075 aluminum alloy composite fabricated by spark plasma sintering, *Int. J. Miner. Metall. Mater.*, 27(2020), No. 9, p. 1295.

[12] J.Y. Wang, Y.C. Zhou, T. Liao, J. Zhang, and Z.J. Lin, A first-principles investigation of the phase stability of $Ti_2AlC$ with Al vacancies, *Scripta Mater.*, 58(2008), No. 3, p. 227.

[13] H. Wang, H. Han, G. Yin, *et al.*, First-principles study of vacancies in $Ti_3SiC_2$ and $Ti_3AlC_2$, *Materials*, 10(2017), No. 2, art. No. 103.

[14] W.B. Yu, X.J. Wang, H.B. Zhao, *et al.*, Microstructure, mechanical properties and fracture mechanism of $Ti_2AlC$ reinforced AZ91D composites fabricated by stir casting, *J. Alloys Compd.*, 702(2017), p. 199.

[15] S. Amini, J.M.C. Gallego, L. Daemen, *et al.*, On the stability of Mg nanograins to coarsening after repeated melting, *Nano Lett.*, 9(2009), No. 8, p. 3082.

[16] B. Anasori, S. Amini, V. Presser, and M.W. Barsoum, Nanocrystalline Mg-matrix composites with ultrahigh damping properties, [in] *Magnesium Technology 2011*, Springer, Cham, 2011, p. 463.

[17] W.B. Yu, X.B. Li, M. Vallet, and L. Tian, High temperature damping behavior and dynamic Young's modulus of magnesium matrix composite reinforced by $Ti_2AlC$ MAX phase particles, *Mech. Mater.*, 129(2019), p. 246.

[18] W.B. Yu, D.Q. Chen, L. Tian, H.B. Zhao, and X.J. Wang, Self-lubricate and anisotropic wear behavior of AZ91D magnesium alloy reinforced with ternary $Ti_2AlC$ MAX phases, *J. Mater. Sci. Technol.*, 35(2019), No. 3, p. 275.

[19] J. Liu, J. Binner, and R. Higginson, Dry sliding wear behaviour of co-continuous ceramic foam/aluminium alloy interpenetrating composites produced by pressureless infiltration, *Wear*, 276-277(2012), p. 94.

[20] C. Lei, Y. Zhou, H.X. Zhai, *et al*., Thermal shock behavior of co-continuous $TiC_x$–Cu cermets in air and anaerobic environment, *Ceram. Int.*, 47(2021), No. 12, p. 16422.
[21] C. Lei, H.X. Zhai, Z.Y. Huang, *et al*., Fabrication, microstructure and mechanical properties of co-continuous $TiC_x$/Cu–$Cu_4Ti$ composites prepared by pressureless-infiltration method, *Ceram. Int.*, 45(2019), No. 3, p. 2932.
[22] M. Pavese, M. Valle, and C. Badini, Effect of porosity of cordierite preforms on microstructure and mechanical strength of co-continuous ceramic composites, *J. Eur. Ceram. Soc.*, 27(2007), No. 1, p. 131.
[23] H.J. Wang, Z.Y. Huang, J.C. Yi, *et al*., Microstructure and high-temperature mechanical properties of co-continuous ($Ti_3AlC_2$+$Al_3Ti$)/2024Al composite fabricated by pressureless infiltration, *Ceram. Int.*, 48(2022), No. 1, p. 1230.
[24] C.L. Zhou, X.Y. Wu, T.L. Ngai, L.J. Li, S. Ngai, and Z.M. Chen, Al alloy/$Ti_3SiC_2$ composites fabricated by pressureless infiltration with melt-spun Al alloy ribbons, *Ceram. Int.*, 44(2018), No. 6, p. 6026.
[25] D.A.H. Hanaor, L. Hu, W.H. Kan, *et al*., Compressive performance and crack propagation in Al alloy/$Ti_2AlC$ composites, *Mater. Sci. Eng. A*, 672(2016), p. 247.
[26] W.B. Yu, W.Z. Jia, F. Guo, *et al*., The correlation between N deficiency and the mechanical properties of the $Ti_2AlN_y$ MAX phase, *J. Eur. Ceram. Soc.*, 40(2020), No. 6, p. 2279.
[27] J.R. Cahoon, W.H. Broughton, and A.R. Kutzak, The determination of yield strength from hardness measurements, *Metall. Trans.*, 2(1971), No. 7, p. 1979.
[28] S.J. Zinkle, D.H. Plantz, A.E. Bair, R.A. Dodd, and G.L. Kulcinski, Correlation of the yield strength and mlcrohardnesss of high-strength, high-conductivity copper alloys, *J. Nucl. Mater.*, 133-134(1985), p. 685.
[29] L. Vandeperre and W.J. Clegg, The correlation between hardness and yield strength of hard materials, *Mater. Sci. Forum*, 492-493(2005), p. 555.
[30] S.B. Li, W.B. Yu, H.X. Zhai, G.M. Song, W.G. Sloof, and S.V.D. Zwaag, Mechanical properties of low temperature synthesized dense and fine-grained $Cr_2AlC$ ceramics, *J. Eur. Ceram. Soc.*, 31(2011), No. 1-2, p. 217.
[31] B. Anasori, E.N. Caspi, and M.W. Barsoum, Fabrication and mechanical properties of pressureless melt infiltrated magnesium alloy composites reinforced with TiC and $Ti_2AlC$ particles, *Mater. Sci. Eng. A*, 618(2014), p. 511.
[32] K. Kozak, M.M. Bućko, L. Chlubny, J. Lis, G. Antou, and T. Chotard, Influence of composition and grain size on the damage evolution in MAX phases investigated by acoustic emission, *Mater. Sci. Eng. A*, 743(2019), p. 114.
[33] C.L. Yang, B. Zhang, D.C. Zhao, *et al*., Microstructure evolution of as-cast AlN/AZ91 composites and room temperature compressive properties, *J. Alloys Compd.*, 774(2019), p. 573.
[34] R.O. Ritchie, The conflicts between strength and toughness, *Nat. Mater.*, 10(2011), No. 11, p. 817.
[35] W. Yu, V. Mauchamp, T. Cabioc'h, *et al*., Solid solution effects in the $Ti_2Al(C_xN_y)$ MAX phases: Synthesis, microstructure, electronic structure and transport properties, *Acta Mater.*, 80(2014), p. 421.
[36] W.J. Wang, V. Gauthier-Brunet, G.P. Bei, *et al*., Powder metallurgy processing and compressive properties of $Ti_3AlC_2$/Al composites, *Mater. Sci. Eng. A*, 530(2011), p. 168.